Proceedings of ASME Turbo Expo 2025
Turbomachinery Technical Conference and Exposition
GT2025
June 16 – 20, 2025, Memphis, Tennessee

GT2025-153268

REDUCING NOx EMISSIONS IN AMMONIA COMBUSTORS

Satyendra Rana
University of Connecticut, Storrs, CT, 06269, USA

Paul Papas*
RTX Technology Research Center, East Hartford, CT, 06118, USA

Lance L. Smith
RTX Technology Research Center, East Hartford, CT, 06118, USA

Chih-Jen Sung
University of Connecticut, Storrs, CT, 06269, USA

ABSTRACT

Ammonia continues to attract growing interest as a carbon-neutral replacement fuel, motivating numerous research efforts toward understanding fundamental ammonia combustion characteristics. A major challenge for the use of ammonia is the development of combustor technologies for mitigating potentially high NOx emissions from the fuel-bound nitrogen chemical pathways to acceptable levels. Our work focuses on a staged RQL combustor architecture for minimizing the NOx emission levels through burning fuel-rich in the primary stage to form combustion products containing significant levels of hydrogen in addition to nitrogen and water with minimal NOx formation. The subsequent quench and burnout stages of the combustor must then quickly burn residual hydrogen with flame-temperatures moderated by nitrogen and water forming in the first stage. Chemical Reactor Network modeling was used to understand and identify optimal stoichiometry and residence times in each stage for minimizing NOx emissions and to quantify pressure and temperature effects. Reducing the overall NOx emissions requires relatively long residence times in the primary stage to achieve near equilibrium NO levels due to kinetically controlling processes. For conditions relevant to gas turbines (e.g., 30 atm), our work indicates that NOx emissions below 20 ppm are theoretically achievable in a staged RQL combustor architecture. However, these emission predictions significantly depend on the accuracies of currently available chemical kinetic mechanisms which have not been extensively validated under elevated pressure and temperature conditions relevant to gas turbines.

Keywords: Ammonia combustion, NOx emission, chemical reactor network modeling

*Corresponding author: paul.papas@rtx.com

NOMENCLATURE

τ	Residence time, [ms]
ϕ_r	Rich-stage equivalence ratio, [−]
ϕ_l	Lean-stage equivalence ratio, [−]
C_{ji}^{d}	Normalized destruction of the j^{th} species of the i^{th} reaction, [−]
C_{ji}^{p}	Normalized production of the j^{th} species of the i^{th} reaction, [−]
E_{ji}	Normalized sensitivity coefficient of the j^{th} species of the i^{th} reaction, [−]
P_{in}	Inlet pressure, [atm]
T_{in}	Inlet temperature, [K]
T_{out}	Outlet temperature, [K]

1. INTRODUCTION

Ammonia-fueled combustors are increasingly explored as a means to reduce carbon emissions in gas turbines, given ammonia's potential as a carbon-free alternative to hydrocarbon fuels. However, one of the key challenges associated with the combustion of ammonia in gas turbines is the emission of nitrogen oxides (NOx), which in the atmosphere react with water vapor and solar radiation to form nitric acid, a component of acid rain, and ground level ozone, a component of smog. To achieve key performance metrics such as efficiency, ultra-low NOx emissions, and stability in both low- and high-power conditions, the *rich-burn/quick-quench/lean-burn* (RQL) combustor design for aircraft turbines is firmly established [1, 2]. Although the RQL design was initially developed for hydrocarbon fuels and their blends with low heating value fuels [3–7], it is now increasingly being explored as a potential option for ammonia combustion [8–10].

The two most significant parameters that influence both power performance requirements and NOx formation in an NH_3-fired gas turbine are the equivalence ratio and the residence time of the fuel-air mixture. In the RQL design, combustion is initiated

in the fuel-rich primary zone (front-end) and the fuel-air mixture is quickly reacted and diluted (quenched) with additional airflow in the secondary zone (downstream section) of the combustor to reach the fuel-lean conditions at the combustor exit. The concept underlying the RQL combustor for NH_3 combustion is depicted in Figures 1a and 1b, which are described further below in the context of emissions and how NH_3 chemical kinetics determine the approach to equilibrium levels. All simulation results shown in these figures for NH_3 combustion are performed using the Stagni mechanism [11].

The initial fuel-rich combustion process, denoted as "Rich Burn" in Figure 1a, effectively suppresses NOx formation by limiting the availability of oxygen for NOx formation, resulting in oxygen preferentially being consumed to form the low-energy product species H_2O rather than NOx. To illustrate the important effects of equivalence ratio and residence time, Figure 1a shows the computed peak NO levels in adiabatic freely propagating flames for conditions relevant to gas turbine combustors – 35 atm and initial reactant temperature of 850 K. The peak NO concentrations within the flame zones at these conditions drop precipitously with increasing equivalence ratio (ϕ) on the rich side, and increasing residence time (τ) in the post-flame region towards lower equilibrium levels. For a flame residence time of about 40 ms from the maximum heat release location, the local NO concentration within the post-flame zone already drops to near equilibrium levels.

Figure 1b plots the variation for the NH_3 concentration with equivalence ratio in comparison to equilibrium NO and NH_3 levels. As the equivalence ratio increases, the NO levels decrease, whereas the NH_3 levels in the post-flame zone increase with rising ϕ. At a residence time of 40 ms in the post-flame region, the local NH_3 levels correspond closely with equilibrium levels until about $\phi = 1.5$, beyond which local NH_3 levels significantly exceed equilibrium concentrations. Subsequently, the optimum combustor performance in terms of overall equivalence ratio for lowest emissions manifests from the trade between NO reduction and NH_3 slippage, and Figure 1b shows that this optimum occurs in the vicinity of $\phi = 1.4$. Consequently, in the fuel-lean secondary zone for RQL-type architectures, NOx concentrations rise because of elevated temperatures and the presence of unburned NH_3 along with abundance of O/H radicals and available oxygen. Additionally, the emissions in both the primary and secondary zones are also affected by the residence time of the fuel-air mixture. While the optimal operating conditions for low NOx emissions in RQL-type, gas turbine combustors using hydrocarbon fuels are relatively well established, the ideal conditions for NH_3-fired systems to minimize NOx emissions – such as equivalence ratio, pressure, exit temperature, and residence time – are an area of active research. A deeper understanding of ammonia combustion kinetics is essential to determine the optimal conditions for reducing NOx emissions in high-pressure turbine operations [10, 12, 13].

The chemical kinetic studies and validation of RQL-staged combustion strategy in terms of pollutant predictions can be accomplished using the widely adopted chemical reactor network (CRN) method. Several recent studies [14–16] have confirmed the effectiveness of the RQL design approach for the combustion

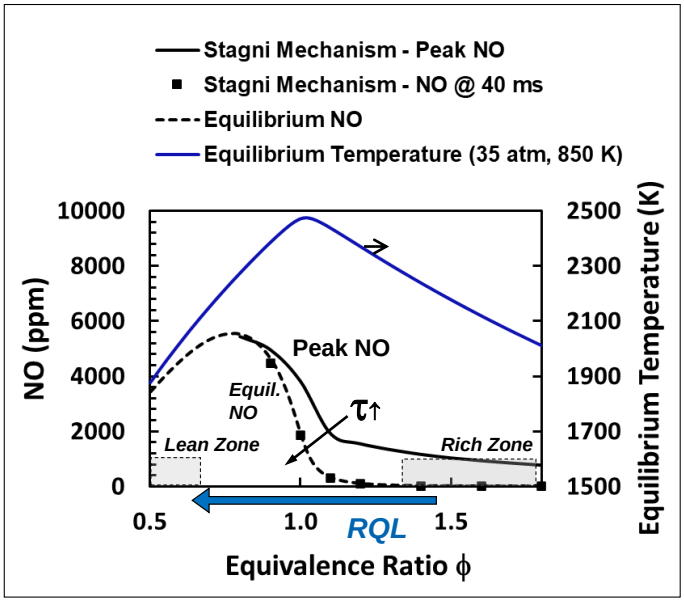

(a)

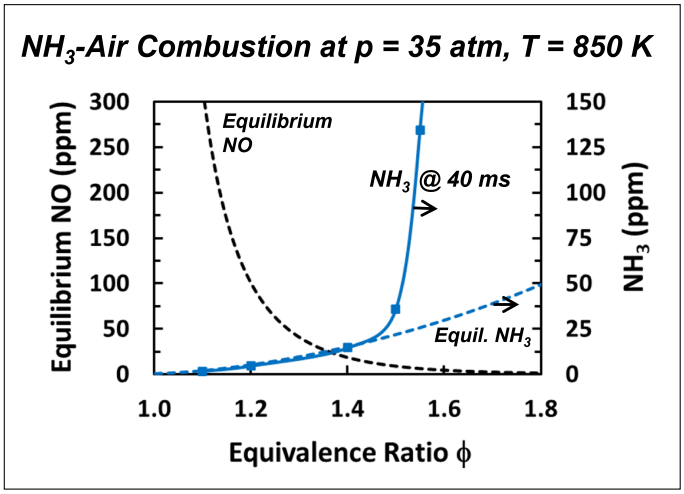

(b)

FIGURE 1: Illustration of pollutant species NH_3 and NO at varying equivalence ratios, showing basis for RQL combustion of pure NH_3 fuel with low NOx emissions. (a) Concentration of peak NO in flame at <1 ms from maximum heat release location (solid black line); NO concentration in flame at 40 ms from maximum heat release location (solid black square symbols); and NO concentration at equilibrium (dashed line). Equilibrium temperature (adiabatic flame temperature) is shown using the right-hand axis. (b) Concentration of NH_3 illustrated using the right-hand axis, with the solid blue line indicating NH_3 concentration after 40 ms from maximum heat release location, and the dashed blue line indicating NH_3 concentration at equilibrium. All values are calculated by the authors using the Stagni mechanism [11] for ammonia combustion, for ammonia-air freely propagating premixed flames at 850 K inlet temperature and 35 atm pressure.

of NH_3 and its blends with other fuels through the application of CRN modeling. Gubbi *et al.* [14] used a two-stage reactor network model comprised of freely propagating flame models in

combination with perfect mixers to evaluate the theoretical minimum achievable NO emissions for constrained combustor exit H_2 values. By determining the minimum NO concentrations, they identified the optimal fuel-rich stage equivalence ratio (ϕ_r) and fuel-lean stage residence time for a given total residence time. Their studies predicted a monotonic increase in NO concentrations at the combustor exit with increasing fuel-lean stage residence times, at all temperatures. Additionally, their research indicates that an increase in pressure will monotonically decrease total NO levels at the combustor exit for a given temperature.

Li *et al.* [15, 16] used two-stage CRN modeling to elucidate the effects of oxygen enrichment and hydrogen addition on NOx emissions for NH_3 combustion in a typical E-class turbine at a given design pressure, as well as inlet and outlet temperatures. Their studies showed that the rich-stage equivalence ratio is the primary factor in minimizing NOx emissions. The concentrations of NH_i and OH/H radicals in the rich-stage determine the dominant mechanisms for NO formation and destruction. However, the aforementioned studies lack a systematic and parametric analysis of the effects of residence times, pressure, temperature, and NH_3-slip on NOx formation under gas turbine conditions. Moreover, they lack essential reaction path and sensitivity analyses for a range of gas turbine design parameters required to optimize the design for ammonia combustion. These chemical kinetic analyses are crucial for devising strategies to enhance turndown and reduce NOx emissions in ammonia-air combustors.

This study aims to address this gap by further investigating NOx emission control mechanisms in RQL combustors using CRN modeling. It involves the CRN simulations for varied combustion parameters relevant to gas turbines to investigate effects of varying equivalence ratio and residence times in the rich and lean stage, exit temperature, and design pressure on the NOx concentration. Additionally, rate-of-production and sensitivity analyses were performed to identify the major reaction pathways critical to production or consumption of NOx and NH_3 at critical instants in the reactor network.

2. MODELING

The chemical reactor network modeling method is widely used for the chemical kinetic studies of NOx emissions in RQL staged NH_3-fired gas combustor architectures. CRN modeling offers an optimum approach with the detailed chemical kinetics of complex combustion processes and consequently, good accuracy in predicting NOx emissions in gas turbine combustors. In this paper, a CRN modeling study on the NOx emission characteristics for a two-stage RQL ammonia-air combustion was conducted using Cantera [17] and Python interface. Cantera is an open-source flame/chemical kinetics software tool. Simulations for multiple design cases were performed for different combustion parameters to estimate the overall NOx conversion rate under varying conditions.

2.1 Chemical Reactor Network Model

The CRN model consists of a fuel-rich stage and a fuel-lean stage combustion regions, as illustrated in Figure 2. The model consists of a pair of perfectly-stirred (PSR) and plug-flow (PFR) reactors connected in series for both the fuel-rich and fuel-lean

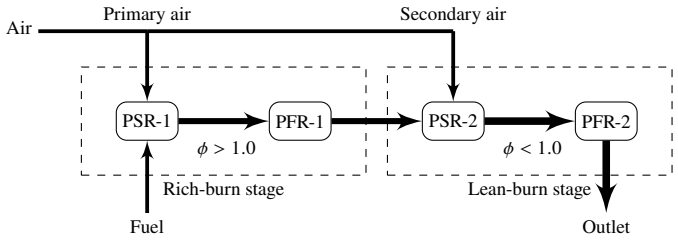

FIGURE 2: The CRN model for a two-stage RQL combustor.

stages. For the fuel-rich stage, a PSR was used to represent the fuel-air mixing and flame anchoring region, whereas a PFR was used to represent the combustion region downstream of the flame anchoring zone. In the case of the fuel-lean stage, quick mixing of the secondary air stream with fuel-rich stage combustion products was modeled using a PSR and the post-mixing combustion was simulated through PFR modeling. Using Cantera's `IdealGasReactor` construct, an adiabatic reactor model at constant pressure was used to simulate the PSR, while the PFR was modelled using `ConstantPressureReactor` class object which is an adiabatic constant-pressure system. To incorporate the thermodynamic properties and reaction rates in the calculation of evolution of species, a mechanism file in `.YAML` format is required for the Cantera transient simulations. Separate gas phase "objects" (using the same mechanism) were created for the fuel-rich and fuel-lean stages to calculate the concentration, rate of production, rate of reaction and other thermodynamic properties of species at each instant of time. Along with the design residence times and inlet temperature and pressure, a range of fuel-rich stage equivalence ratios were selected as input parameters and, the amount of secondary air (and fuel-lean stage equivalence ratio, ϕ_l) was determined by iteration to maintain the given design combustor outlet or exhaust temperature.

2.2 Chemical Kinetic Mechanism

A comparative CRN analysis was conducted through simulation of a particular set of input parameters using various published N/H mechanisms. The four published ammonia mechanisms examined here include Glarborg [18], Powell [19], Mei [20], and Stagni [11]. The results of this analysis are depicted in Figure 3 by plotting NOx as a function of global residence time (τ_g). The NOx concentration at the exit of PFR-2 in these simulations ranges from 12.12 ppm to 13.05 ppm for $\phi_r = 1.45$. In this paper, NOx is defined as the total concentration of NO, NO_2, and N_2O. All the NOx levels have been corrected to dry 15 % vol. O_2. The time scale for NOx reduction at early time in PFR-1 is kinetically driven; as a result, significant variations are expected in this region across different N/H chemical kinetic mechanisms in the literature, as well as in their respective relaxation rates toward equilibrium. Previous work [21, 22] has shown that the Stagni mechanism gives reasonable predictions for laminar flame speeds and counterflow extinction strain rates for NH_3-air flames at elevated pressure. Therefore, the detailed Stagni mechanism with 31 species and 203 reactions was selected here to study the NOx emission characteristics and reaction pathways analyses of NH_3-air combustion.

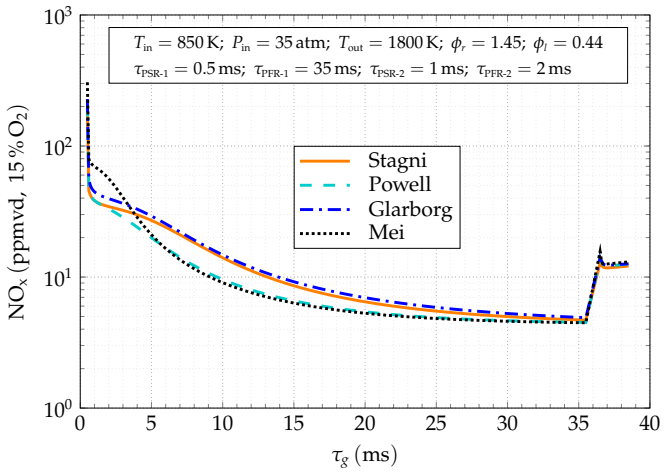

FIGURE 3: Prediction of NOx from different mechanisms for baseline conditions.

2.3 Model Parameters

A parametric study was performed over a range of conditions relevant to gas turbine cycles, including operating pressures, temperatures, and residence times characteristic of a typical aeroderivative cycle. Table 1 provides the combustion parameters used for simulating the various study sets considered in this study. The *baseline* combustor inlet conditions were selected as P_{in} = 35 atm and T_{in} = 850 K to be representative of an aeroderivative gas turbine [23], and the *baseline* combustor exit temperature was selected as T_{out} = 1800 K (with ±100 K case variations) to be representative of low-NOx combustor design practice in both aeroderivative and frame engines [24]. In addition, the mixing residence times for flame-anchoring (τ_{PSR-1} = 0.5 ms) and for secondary-air mixing (τ_{PSR-2} = 1.0 ms) were selected to be consistent with aeroderivative engine design practice [2]. By definition, each perfectly stirred reactor model assumes an ideal steady-state reactor with instantaneous and perfectly uniform concentrations throughout the control volume. In contrast, a plug-flow reactor represents a one-dimensional, steady-state ideal reactor with varying concentrations along the spatial coordinate in our CRN model. In all results reported here, a residence time of 0 ms corresponds to the beginning of PSR-1.

Initial simulations suggest that the optimal NOx emissions at the RQL system outlet are significantly influenced by the residence time in the PFR-1, as shown in Figure 4. The trend lines in the figure correspond to a total of 16 simulations for a range of total residence times. These simulation lines are grouped based on τ_{PFR-1} = 5 ms, 10 ms, 15 ms, and 20 ms under baseline conditions, with τ_{PFR-2} = 5 ms, resulting in overlapping plotted lines within each group. These initial simulations also indicate that the optimum (corresponding to minimum NOx emission) rich-stage equivalence ratio increases with total residence time, ranging from 1.30 to 1.45. Therefore, a range of residence time for PFR-1 was selected to investigate its effect on NOx concentration in additional simulations. The range of conditions for these additional simulations are shown in Table 1.

TABLE 1: Combustion parameters used in the CRN modeling. Highlighted areas are the key parametric changes.

Study set	τ_{total} (ms)	τ_{PSR-1} (ms)	τ_{PFR-1} (ms)	τ_{PSR-2} (ms)	τ_{PFR-2} (ms)	P_{in} (atm)	T_{in} (K)	T_{out} (K)	ϕ_r (-)
A	38.5	0.5	35	1	2	35	850	1800	1.0 – 1.8
B	11.5 – 41.5	0.5	5 – 35	1	2 – 5	35	850	1700	1.0 – 1.8
C	11.5 – 41.5	0.5	5 – 35	1	2 – 5	35	850	1800	1.0 – 1.8
D	11.5 – 41.5	0.5	5 – 35	1	2 – 5	35	850	1900	1.0 – 1.8
E	11.5 – 41.5	0.5	5 – 35	1	2 – 5	20	850	1800	1.0 – 1.8
F	11.5 – 41.5	0.5	5 – 35	1	2 – 5	30	850	1800	1.0 – 1.8
G	11.5 – 41.5	0.5	5 – 35	1	2 – 5	40	850	1800	1.0 – 1.8

3. RESULTS AND DISCUSSIONS

The following section systematically presents the simulation results, highlighting the influence of various operational parameters on NOx emissions in the RQL combustor. Parameters such as equivalence ratio, design pressure, exit or outlet temperature, and residence time are examined to determine the contributions to NOx formation.

Table 2 summarizes the results of selected simulations. In all cases, the residence times for PSR-1 and PSR-2 are 0.5 ms and 1.0 ms, respectively. Additionally, in all cases, the concentration of NH_3 decreases significantly from the rich-stage to the lean-stage. Cases A1 and A2 illustrate the considerable increase in NH_3-slip and NOx concentrations in the rich and lean stages, respectively, due to an increase in the rich-stage equivalence ratio from 1.45 to 1.80. In Cases C1 to G2, the listed ϕ_r values are the optimal equivalence ratio ($\phi_{r,opt}$) values yielding the corresponding minimum NOx emission values. The effects of exit temperature and residence times on NH_3-slip and NOx concentration are demonstrated by Cases C1 to D2. Cases C1 and C2 show that, at the same exit temperature, increasing the residence time of PFR-1 reduces the NOx concentration at the exit of PFR-2. A comparison of Cases C2 and D1 reveals that both NOx

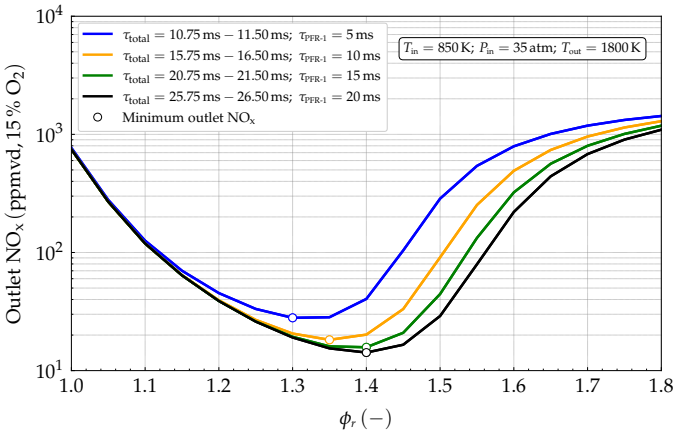

FIGURE 4: Effects of residence times and rich-stage equivalence ratio on prediction of NOx at the outlet. The simulations are presented for a range of total residence times under baseline conditions, grouped by τ_{PFR-1} = 5 ms, 10 ms, 15 ms, and 20 ms.

TABLE 2: Summary of results from selected simulations. Highlighted areas are the key parametric changes.

								Rich Stage[#]		Lean Stage[§]	
Case	τ_{total} (ms)	τ_{PFR-1} (ms)	τ_{PFR-2} (ms)	P_{in} (atm)	T_{out} (K)	ϕ_r (-)	ϕ_l[‡] (-)	NH_3[†] (ppm)	NOx* (ppm)	NH_3[†] (ppb)	NOx* (ppm)
A1	38.5	35	2	35	1800	1.45	0.45	17.5	4.7	0.023	12.1
A2	38.5	35	2	35	1800	1.80	0.45	6384.3	2.6	0.013	895.4
A3	38.5	35	2	35	1800	1.10	0.45	1.7	120.4	0.021	118.3
C1	11.5	5	5	35	1800	1.30	0.45	12.6	23.2	0.022	28.3
C2	41.5	35	5	35	1800	1.45	0.45	17.5	4.6	0.023	12.9
D1	41.5	35	5	35	1900	1.45	0.51	17.5	4.6	0.073	19.4
D2	38.5	35	2	35	1900	1.45	0.51	17.5	4.6	0.073	15.3
E1	11.5	5	5	20	1800	1.35	0.45	14.7	36.2	0.017	40.0
E2	41.5	35	5	20	1800	1.45	0.45	10.5	6.5	0.018	11.9
G1	11.5	5	5	40	1800	1.30	0.45	13.7	20.3	0.024	26.2
G2	41.5	35	5	40	1800	1.40	0.45	15.4	6.0	0.024	13.4

[#] At the end of fuel-rich stage
[§] At the end of fuel-lean stage
[‡] Lean-stage equivalence ratio is same as global equivalence ratio
[†] Wet basis
* 15 % O_2 dry basis

and NH_3-slip increase at the exit of PFR-2 with a rise in exit temperature. Note that the NH_3 concentrations at the lean-stage exit are negligigle for all cases, and are reported in the table as parts per billion. Furthermore, increasing the residence time of PFR-2 leads to a higher NOx concentration at the combustor exit, as shown by the data for Cases D1 and D2. A comparison of Cases E1 and E2 shows that, at the same design pressure, NOx concentration at the combustor exit decreases with an increase in the residence time of PFR-1. The impact of pressure and residence times on NH_3-slip and NOx concentration is illustrated by Cases E1 to G2. For a given total residence time, increasing the design pressure leads to a significant decrease in exit NOx concentration for short τ_{PFR-1}, as shown by the comparison of Cases E1 and G1. By increasing the τ_{PFR-1} from 5 ms to 35 ms, which in turn increase the total residence time from 11.5 ms to 41.5 ms, the NOx emission levels of E2 and G2 are substantially reduced in comparison to E1 and G1. However, for E2 and G2, the increase in operating pressure results in a minor increase in outlet NOx concentration. A more detailed discussion on these trends is provided in Section 3.3.

In addition to the above parametric variations, this study will also examine the rate of production and consumption analysis, sensitivity analysis, and the role of reaction pathways that influence NOx formation and NH_3 concentration under various operating conditions.

3.1 Dependence of Rich-Stage Equivalence ratio

To investigate the impact of the rich-stage equivalence ratio on NOx emissions, ϕ_r was varied between 1.0 and 1.8, while the combustor exit temperature was maintained at a constant value by adjusting the secondary air flow into the second stage. Figure 5 shows the variation of NOx and NH_3 concentrations throughout the Chemical Reactor Network as a function of the global residence time for the baseline case for selected rich-stage equivalence ratios. Again, all the NOx emission levels have been

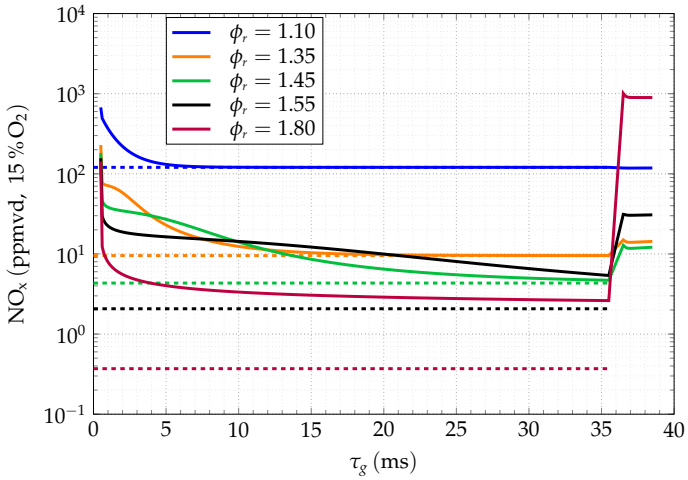

(a) Evolution of NOx with global residence time

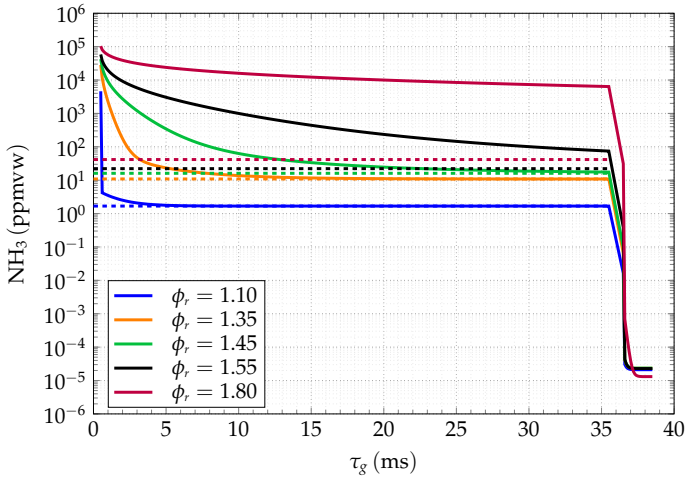

(b) Evolution of NH_3 with global residence time

FIGURE 5: Evolution of NOx and NH_3 with global residence time in the combustor for baseline conditions (P_{in} = 35 atm, T_{in} = 850 K, T_{out} = 1800 K, τ_{PSR-1} = 0.5 ms, τ_{PFR-1} = 35.0 ms, τ_{PSR-2} = 1.0 ms, and τ_{PFR-2} = 2.0 ms). The dashed lines show the equilibrium NOx or NH_3 for the corresponding rich-stage equivalence ratio.

corrected to dry 15 % vol.O_2. At the start of the PFR-1 reactor, a rapid decrease in NOx concentration is observed for all rich-stage equivalence ratios, with the initial decay rate increasing as the equivalence ratio is increased. In contrast, while a rapid decrease in NH_3 concentration is also observed in PFR-1 for all rich-stage equivalence ratios, the initial NH_3 decay rate decreases as the equivalence ratio is increased. Figures 5a and 5b show a rapid increase in NOx concentrations and a decrease in NH_3 concentrations at the end of PSR-2, respectively in the reactor network across all ϕ_r, following the introduction of secondary air. For the conditions examined, the maximum and minimum concentrations of NOx at the combustor exit were observed at $\phi_r = 1.80$ and $\phi_r = \phi_{r,\,opt} = 1.45$, respectively. The increased NOx formation for

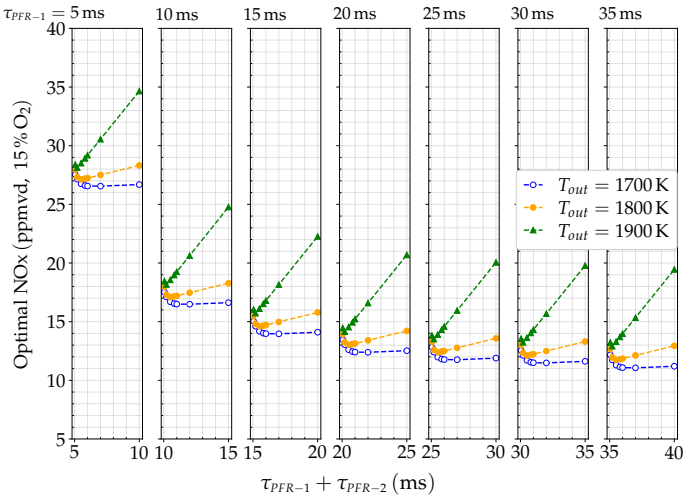

FIGURE 6: Effects of exit temperature on optimal NOx levels for different combinations of τ_{PFR-1} and τ_{PFR-2}. The figure shows a collection of several individual graphs, where in each subplot, τ_{PFR-2} varies from 0.05 ms to 5 ms for a given value of τ_{PFR-1}, indicated at the left edge of each subplot. τ_{PFR-1} ranges from 5 ms to 35 ms across the subplots. The conditions are: P_{in} = 35 atm, T_{in} = 850 K, τ_{PSR-1} = 0.5 ms, and τ_{PSR-2} = 1.0 ms.

$\phi_r > \phi_{r,\,opt}$ can be attributed to increased NH_3-slip and fuel NOx pathways in the fuel-lean stage. The dashed lines, which extend only to the end of the fuel-rich stage (τ_g = 35.5 ms) for each case, represent the equilibrium NOx or NH_3 for the rich-stage equivalence ratio. These equilibrium NOx emission levels have also been corrected to dry 15 % vol.O_2. As demonstrated in Figure 5b, for $\phi_r > 1.5$, the approach to equilibrium for NH_3 concentration is considerably slower than for $\phi_r < 1.5$. Figure 5a shows that in the NOx-optimal case (ϕ_r = 1.45), NOx levels decline rapidly during the fuel-rich stage as the τ_g in PFR-1 increases, eventually approaching equilibrium NOx concentrations by the end of PFR-1. Additionally, the NOx concentration remains nearly constant between residence times of approximately 25 ms and 35.5 ms in PFR-1. This suggests that the residence time of PFR-1 can be reduced for the optimum case for minimizing NOx emissions. For $\phi_r < 1.45$, the NOx concentrations for each ϕ_r tend to quickly approach their equilibrium values as τ_g increases.

3.2 Dependence of Exit Temperature

Simulations were carried out under baseline conditions to examine the effect of changing the combustor exit temperature on NOx concentration. Figure 6 illustrates the NOx emission levels for the combination of τ_{PFR-1} and τ_{PFR-2} at the outlet temperatures of 1700 K, 1800 K and 1900 K. For each combination of τ_{PFR-1} and τ_{PFR-2}, the residence times of PSR-1 and PSR-2 were fixed at 0.5 ms and 1.0 ms, respectively. The figure presents a compilation of several individual graphs. In each subplot, corresponding to a given τ_{PFR-1}, the optimal NOx is displayed as a function of τ_{PFR-2}, which varies from 0.05 ms to 5 ms. The optimum equivalence ratio for Figure 6 ranges from 1.30 to 1.45 across all the conditions and residence times shown. The lean-stage or overall equivalence ratio corresponding to T_{out} = 1700 K, 1800 K and 1900 K are 0.38, 0.45 and 0.51, respectively. The relatively small increase in ϕ_l is attributed to the decrease in the amount of secondary air added to the lean stage, which increases the exit temperature. The figure illustrates that for all three exit temperatures, NOx concentrations exhibit a slight initial decline, followed by an increase, as the residence time of PFR-2 increases. The rise in NOx concentration over time is most significant for T_{out} = 1900 K, whereas for the other two temperatures (1700 K and 1800 K), the rise is minimal. These results suggest that the residence time in PFR-2 has little to no impact on NOx concentration for $T_{out} < 1800$ K. NOx formation at $T_{out} > 1800$ K is driven by the Zel'dovich mechanism which is controlled in large part by the high activation energy rate-limiting reaction $N_2 + O \rightleftharpoons NO + N$. An increase in temperatures enhances the O/H radical pool by accelerating the temperature-sensitive chain branching reactions. As a result, elevated NOx emission levels is observed in PFR-2 as the residence time increases. Furthermore, the HNO intermediate pathway serves as the primary route for NO formation in NH_3-air flames under all conditions [12]. HNO is primarily converted to NO through its reactions with H, OH, and O_2 as well as via thermal dissociation.

3.3 Dependence of Design Pressure

To evaluate the effect of varying the combustor design pressure, simulations were conducted under baseline conditions with adjustments to the pressure to examine its impact on NOx concentration. Figure 7 presents the NOx emission levels for the combination of τ_{PFR-1} and τ_{PFR-2} at design pressures of 20 atm, 30 atm, and 40 atm. For each combination of τ_{PFR-1} and τ_{PFR-2}, the residence times of PSR-1 and PSR-2 were fixed at 0.5 ms and 1.0 ms, respectively. The figure presents a compilation of several individual graphs. In each subplot, corresponding to a given τ_{PFR-1}, the optimal NOx is displayed as a function of τ_{PFR-2}, which varies from 0.05 ms to 5 ms. The optimum equivalence ratio for Figure 7 ranges from 1.30 to 1.45 across all the conditions and residence times shown. As the residence time in PFR-2 increases, the NOx concentration initially shows a slight decrease, followed by a gradual rise with increase in τ_{PFR-2}. The figure indicates that at shorter τ_{PFR-1}, NOx emissions decrease with increasing design pressure. However, for longer τ_{PFR-1}, a crossover occurs around 25–30 ms, after which NOx emissions become higher at greater pressures. For $\tau_{PFR-1} > 25$ ms, the NOx concentrations do not vary significantly across the simulated design pressure range. The graph illustrates the importance of elevated pressure for reducing NOx emissions in the fuel-rich stage for shorter PFR-1 residence times below about 20 ms. The O/H radical pool is reduced with increasing pressure due to the three-body pressure sensitive reactions $H + OH + M \rightleftharpoons H_2O + M$ and $H + O_2 (+M) \rightleftharpoons HO_2 (+M)$. The former reaction is a chain terminating reaction, whereas the latter results in the formation of less active HO_2 radicals. Consequently, the active O/H radical pool is reduced, leading to a net decrease in NO production at high pressures, while NO consumption rates by NH_i species remain high [12]. As the residence time in PFR-1 increases, the net production rate of NOx increases under fuel-lean conditions and elevated temperatures. This increase is attributed to the combined effects of increased concentrations of O/H/OH radicals, the activation of Zel'dovich mechanism pathways, and

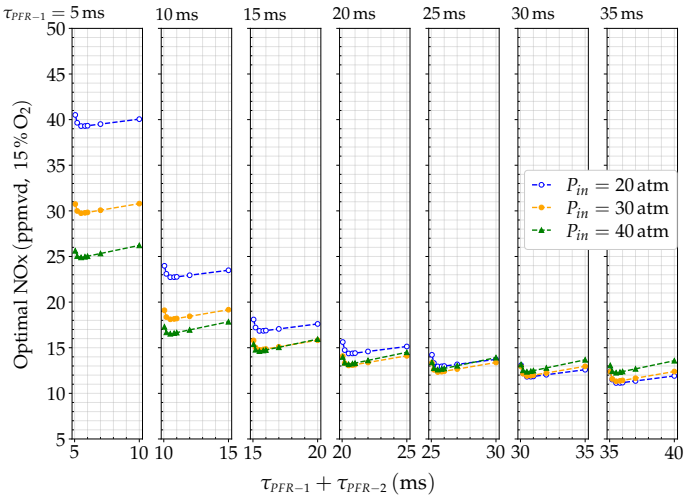

FIGURE 7: Effects of pressure variation on optimal NOx levels for different combinations of τ_{PFR-1} and τ_{PFR-2}. The figure shows a collection of several individual graphs, where in each subplot, τ_{PFR-2} varies from 0.05 ms to 5 ms for a given value of τ_{PFR-1}, indicated at the left edge of each subplot. τ_{PFR-1} ranges from 5 ms to 35 ms across the subplots. The conditions are: T_{in} = 850 K, T_{out} = 1800 K, τ_{PSR-1} = 0.5 ms, and τ_{PSR-2} = 1.0 ms.

the accelerated reaction rates at higher pressures. These effects account for the higher concentration of NOx at 40 atm compared to 20 atm at longer residence times.

3.4 Rate of Production Analysis

A local reaction flow analysis examines the formation and destruction of species at specific points, either in time for time-dependent problems or in space for steady, spatially dependent problems. To examine the primary NOx reaction pathways contributing to its production or destruction in both the rich and lean burn stages, net rate-of-production (ROP) analyses were conducted to identify the dominant NOx reaction steps. As NO is the primary contributor (with N_2O being the second most significant contributor) to NOx concentrations in all simulations, the ROP analysis focuses primarily on NO for brevity. Examples of proportions of NOx constituents are given at the end of Section 3.5. A rate-of-production analysis considers the percentage contributions of different reactions to the formation or destruction of a particular chemical species [25]. The normalized production contribution of a given reaction i to a particular species j for a mechanism that considers N species and L elementary reactions is given by:

$$C_{ji}^{p} = \frac{\max(\nu_{ji} q_i, 0)}{\sum_{i=1}^{L} \max(\nu_{ji} q_i, 0)} \tag{1}$$

The normalized destruction contribution is given by:

$$C_{ji}^{d} = -\frac{\min(\nu_{ji} q_i, 0)}{\sum_{i=1}^{L} \min(\nu_{ji} q_i, 0)} \tag{2}$$

Where, p and d indicates production and destruction of species, ν_{ji} represents the net stoichiometric coefficient of the j^{th} species in the reaction i, and q_i denotes the rate of progress of the i^{th} reaction. A negative sign has been added to the expression for normalized destruction (Equation (2)) to emphasize that it is a consumption reaction.

The effect of rich-stage equivalence ratio on the dominant NO and NH_3 pathways for the baseline conditions is presented in Figures 8 and 9, using normalized production and destruction contribution values. These values are calculated at a critical time instant (τ_g = 0.60 ms) when the rate of change in NO concentration is highest as shown in Figure 5a. To examine the primary reaction pathways for NOx formation and destruction, a comparison was made between ϕ_r = 1.10 and ϕ_r = 1.80 at τ_g = 0.60 ms in Figure 8. At the start of PFR-1 (τ_g = 0.60 ms), the net NO production rate is dominated by HNO (R142, R143, R148) and Zel'dovich (R88) pathways for ϕ_r = 1.80, whereas for ϕ_r = 1.10 the NO_2 reaction (R180) is the main contributor. At the same instant, NO destruction is primarily driven by the Zel'dovich (R90, R88), HNO (R142), and N_2O (R84) pathways for ϕ_r = 1.10. In contrast, for ϕ_r = 1.80, the NH_2 and NH radicals are the main contributors to the destruction of NO concentration. To highlight the interplay between NO formation and unburned NH_3 (slippage), Figure 9 gives the normalized NH_3 production and destruction contributions for important reactions at ϕ_r = 1.10 and ϕ_r = 1.80 near the start of PFR-1 (τ_g = 0.60 ms). The net NH_3 production rate at ϕ_r = 1.10 is primarily governed by the recombination reaction (R23) $NH_2 + H \rightleftharpoons NH_3$, whereas NH_2 recombination and several NH_2/N_2H_i interactions are important at ϕ_r = 1.80. These latter NH_i/N_2H_i chemical interactions are also particularly important for determining the overall rate of reaction for ammonia combustion systems under fuel-rich conditions [19, 22], as well as contribute to the relatively slow NH_3 relaxation to equilibrium shown previously in Figure 1b for $\phi_r > 1.50$. This increased NH_3 slippage explains the increased NOx formation in the fuel-lean stage when air is introduced for $\phi_r > \phi_{r,\,opt}$ due to fuel NOx pathways.

Figure 10 gives the normalized NO production and destruction contributions for important reactions in the fuel-lean stage. Comparisons were made for ϕ_r = 1.45 and ϕ_r = 1.80 at the exit of PSR-2 (τ_g = 36.50 ms). The net NO production rate is primarily governed by the HNO (R147), Zel'dovich (R89), and NO_2 (R180, R181) pathways for both ϕ_r = 1.45 and ϕ_r = 1.80. In contrast, NO destruction is predominantly driven by the NO_2 (R140, R139) pathways in both cases. The abundance of the NH_2 and NH radicals becomes important to destruction of NO in the case of ϕ_r = 1.80.

The relative importance of the major reaction pathways responsible for the production or destruction of NO is also determined through *sensitivity analysis*. This analysis, corresponding to the aforementioned critical time instants under different design conditions, is discussed in the next section.

3.5 Sensitivity Analysis

Sensitivity analyses are used in chemical kinetic studies for identifying the rate-limiting reaction steps and to understand the relative importance of the reactions in the system. This analysis helps determine the effect of uncertainties in parameters and initial conditions on the solution of the set of ordinary differential equations commonly encountered in chemical kinetic studies. It is often convenient, for comparative analysis, to compute normal-

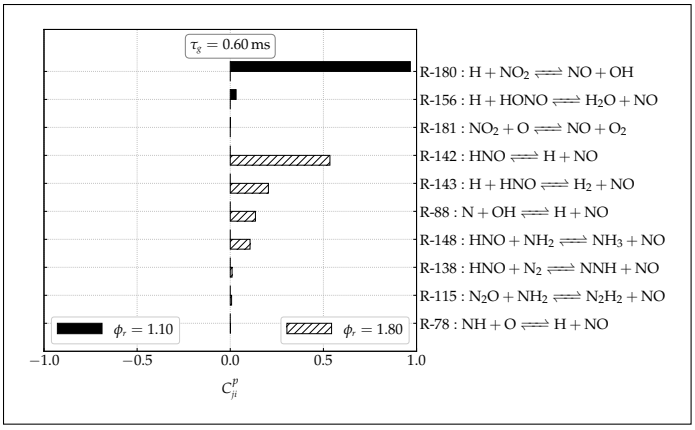

(a) Normalized NO production

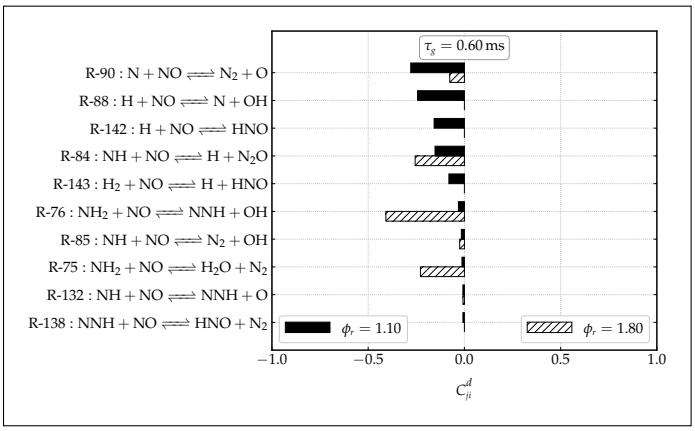

(b) Normalized NO destruction

FIGURE 8: Normalized NO production and destruction contributions of reactions at τ_g = 0.60 ms (beginning of fuel-rich PFR-1 stage) for Cases A3 and A2.

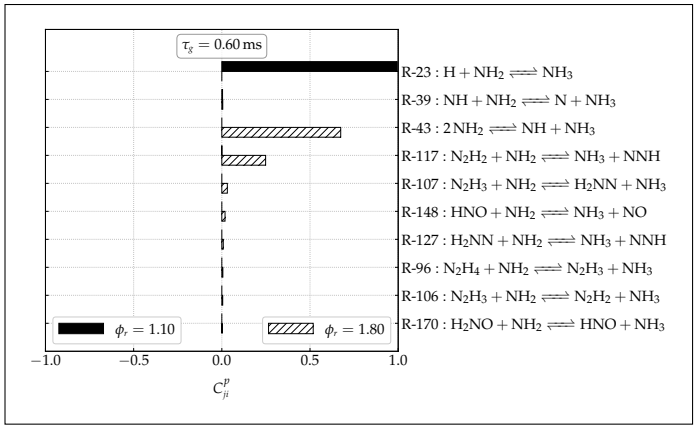

(a) Normalized NH_3 production

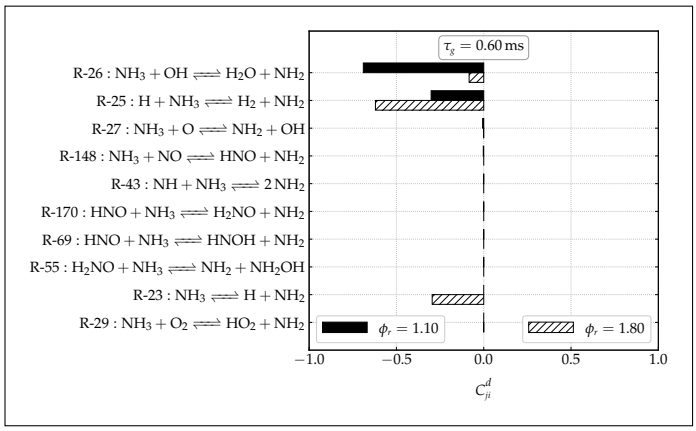

(b) Normalized NH_3 destruction

FIGURE 9: Normalized NH_3 production and destruction contributions of reactions at τ_g = 0.60 ms (beginning of fuel-rich PFR-1 stage) for Cases A3 and A2.

ized sensitivity coefficients as [17, 25–27]:

$$E_{ji} = \frac{\alpha_i}{[\mathrm{M}_j]} \cdot \frac{\partial [\mathrm{M}_j]}{\partial \alpha_i} = \frac{\partial \ln [\mathrm{M}_j]}{\partial \ln \alpha_i} \tag{3}$$

The first-order elementary sensitivities in Equation (3) represents the percentage change in a species concentration ($[\mathrm{M_j}]$) resulting from a percentage change in the parameter α_i at a given τ_g. Normalized sensitivity coefficients are dimensionless and their values are independent of the units of the $[\mathrm{M_j}]$ and α_i. The interpretation of system sensitivity through the first-order elementary sensitivity coefficients is referred to as local sensitivity analysis. In this study, using Cantera, normalized sensitivity coefficients for species NO are determined by varying the forward rate constant of the i^{th} reaction, which inherently affects the backward rate as well due to the equilibrium relationship. This sensitivity accounts for the net effect of both forward and backward rates, as the overall rate of progress in a reversible reaction depends on both.

For the baseline conditions corresponding to simulation output shown in Figure 5a, the local sensitivity coefficients are given in Figure 11 at two critical time instants, where the net destruction and formation rates of NO concentration are highest, respectively. Figure 11a shows that reactions involving $\mathrm{NH_i}$ radicals (R76, R75, R84) have large negative sensitivity coefficients for ϕ_r = 1.80, whereas for ϕ_r = 1.10, the sensitivity magnitude for R84 is much higher than R76 and R75. This suggests that the destruction of NO concentration is very sensitive to rate coefficients of these reactions at τ_g = 0.60 ms (beginning of fuel-rich PFR-1 stage). Additionally, the Zel'dovich pathways R88 and R90 exhibit positive and negative sensitivity coefficients for both equivalence ratios, respectively, emphasizing the role of their kinetic rate constant in the production and destruction of NO. For the fuel-lean PFR-2 stage at τ_g = 36.50 ms and ϕ_r = 1.80 (Figure 11b), NO destruction is predominantly influenced by the R84 (NH + NO $\rightleftharpoons$ H + $\mathrm{N_2O}$) pathway, along with reactions involving $\mathrm{NH_i}$ radicals (R76, R75, R85) and Zel'dovich (R90) pathway. Meanwhile, NO production is primarily governed by the Zel'dovich (R89) and R78 (NH + O $\rightleftharpoons$ H + NO) pathways under the temperature/species conditions at the end of PSR-2. At the same time instant for fuel-lean PFR-2 stage and ϕ_r = 1.45, NO production is sensitive to the reaction rate constant of the $\mathrm{N_2O}$ (R190), Zel'dovich (R90), and NH (R84) pathways. In contrast, NO destruction is primarily influenced by the three-body $\mathrm{NO_2}$ pathway (R140).

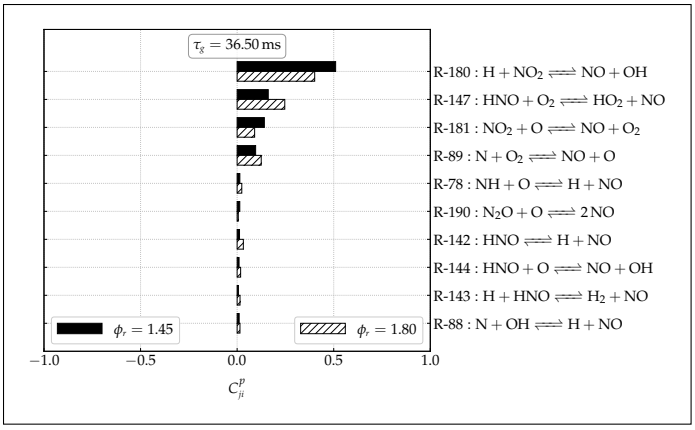

(a) Normalized NO production

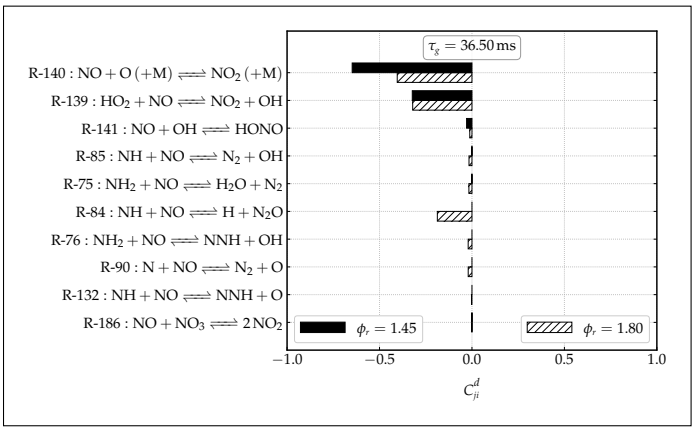

(b) Normalized NO destruction

FIGURE 10: Normalized NO production and destruction contributions of reactions at τ_g = 36.50 ms (end of fuel-lean PSR-2 stage) for Cases A1 and A2.

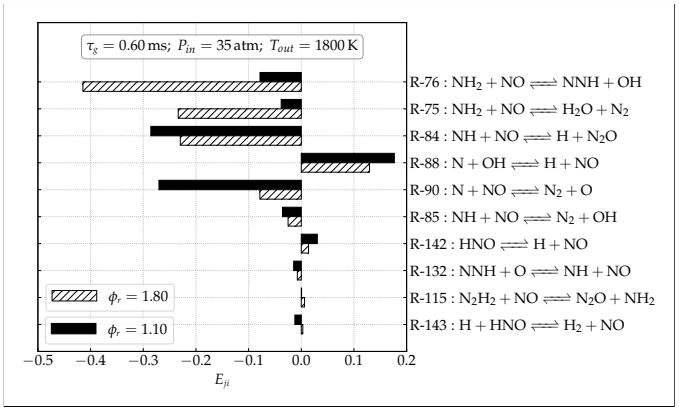

(a) Fuel-rich stage at τ_g = 0.60 ms (beginning of PFR-1)

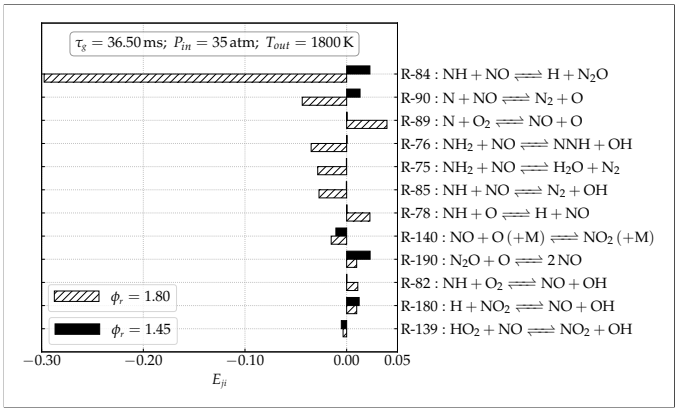

(b) Fuel-lean stage at τ_g = 36.50 ms (end of PSR-2)

FIGURE 11: Normalized sensitivity coefficients for NO for: (a) fuel-rich stage of Cases A3 and A2, (b) fuel-lean stage of Cases A1 and A2.

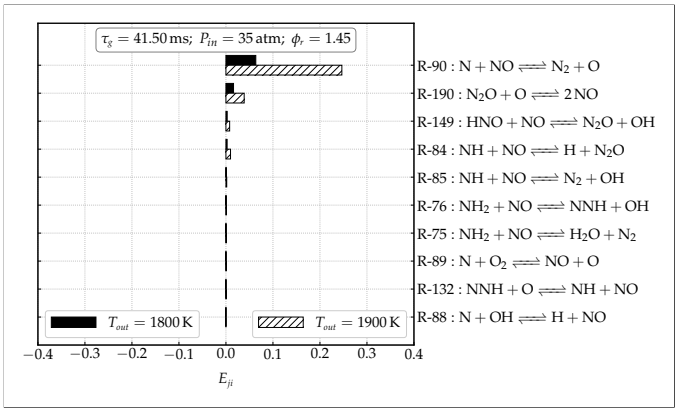

FIGURE 12: Normalized sensitivity coefficients for NO for different exit temperatures at τ_g = 41.50 ms (end of fuel-lean PFR-2 stage) for Cases C2 and D1.

The sensitivity coefficients for NO formation at the end of the fuel-lean PFR-2 stage, corresponding to simulations conducted under different exit temperature conditions shown in Figure 6, are presented in Figure 12. For both temperature values (1800 K and 1900 K), the Zel'dovich pathway (R90) exhibits the highest positive sensitivity coefficients, with the values at 1900 K being significantly larger than those at 1800 K. Thus, the rate constant for the high activation energy step (N_2 + O ⇌ NO + N) in the Zel'dovich mechanism plays a critical role in NO production under the given thermodynamic conditions in the fuel-lean PFR-2 stage. The same trend of higher sensitivity values at elevated temperatures is observed for N_2O and HNO reactions (R190, R149, R84, R85) as well.

The sensitivity coefficients for NO production and destruction at the end of the fuel-rich PFR-1 and fuel-lean PFR-2 stages, corresponding to simulations conducted under different design pressure conditions shown in Figure 7, are presented in Figures 13 and 14. The results correspond to the respective $\phi_{r,\,opt}$ for Cases E1 and G1 with shorter $\tau_{PFR\text{-}1}$ = 5 ms (Figure 13), as well as for Cases E2 and G2 with long $\tau_{PFR\text{-}1}$ = 35 ms (Figure 14). At the end of the fuel-rich PFR-1 stage for short $\tau_{PFR\text{-}1}$, Figure 13a shows that NH_i radical pathways (R76, R84, R75, R85) and the Zel'dovich pathway (R90) exhibit negative sensitivity coefficients for NO. These sensitivity coefficients are comparable at P_{in} = 20 atm and P_{in} = 40 atm. In contrast, for long $\tau_{PFR\text{-}1}$, Figure 14a illustrates that NH_i radical pathways (R76, R84, R75, R85) along with the Zel'dovich pathway (R90) exhibit larger negative sensitivity co-

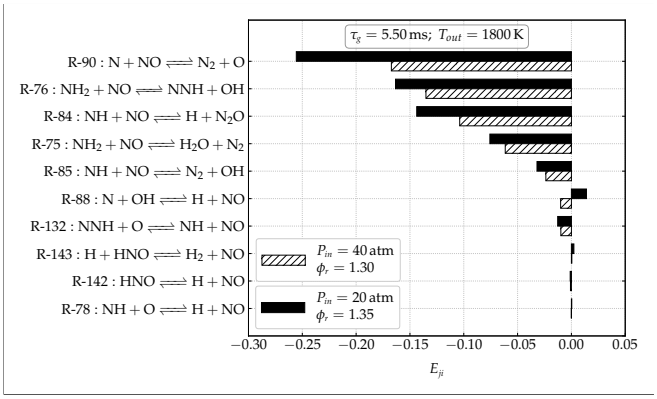

(a) Fuel-rich stage at τ_g = 5.50 ms (end of PFR-1)

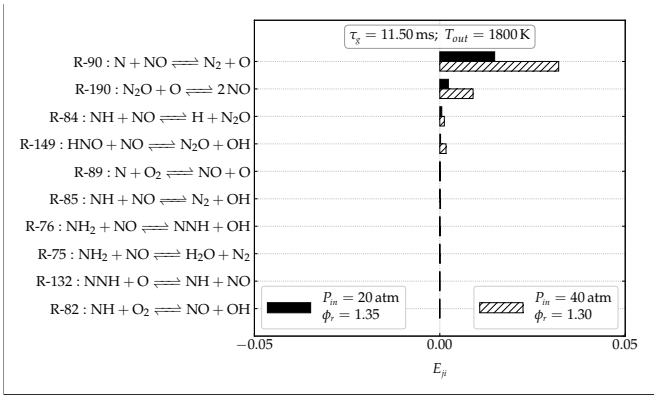

(b) Fuel-lean stage at τ_g = 11.50 ms (end of PFR-2)

FIGURE 13: Normalized sensitivity coefficients for NO at different design pressures for short $\tau_{\text{PFR-1}}$ of 5 ms for Cases E1 and G1.

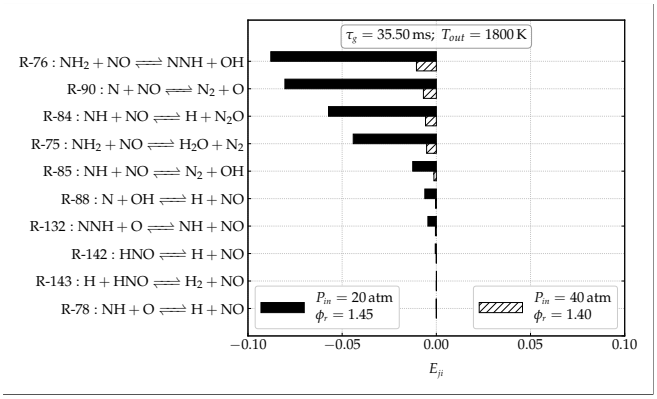

(a) Fuel-rich stage at τ_g = 35.50 ms (end of PFR-1)

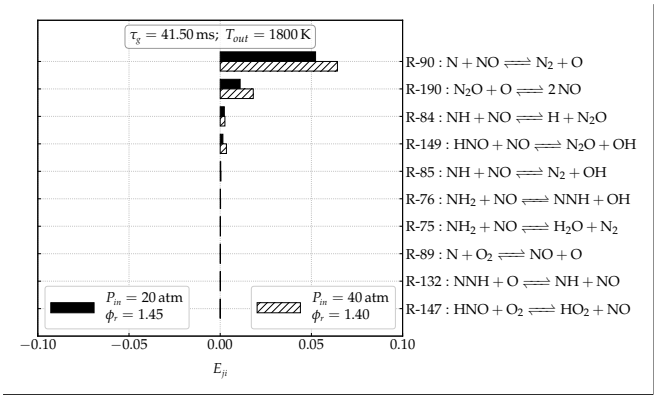

(b) Fuel-lean stage at τ_g = 41.50 ms (end of PFR-2)

FIGURE 14: Normalized sensitivity coefficients for NO at different design pressures for long $\tau_{\text{PFR-1}}$ of 35 ms for Cases E2 and G2.

efficients at $P_{\text{in}} = 20$ atm compared to $P_{\text{in}} = 40$ atm, highlighting the greater influence of their rate constants on NO formation under the lower pressure condition.

At the end of fuel-lean PFR-2 stage, Figures 13b and 14b show that, for both short and long $\tau_{\text{PFR-1}}$, the Zel'dovich pathway (R90) exhibits the highest positive sensitivity coefficients for both 20 atm and 40 atm pressure conditions. For short $\tau_{\text{PFR-1}}$, the relative proportions for NOx at combustor outlet for the design pressure of 20 atm are given by NO : N_2O : NO_2 = 94.62 % : 4.64 % : 0.74 %, whereas the corresponding percentages for 40 atm are 93.3 % : 5.7 % : 1.0 %. Similarly, for long $\tau_{\text{PFR-1}}$, the relative proportions for NOx at combustor exit for the design pressure of 20 atm are given by NO : N_2O : NO_2 = 97.8 % : 0.8 % : 1.4 %, whereas the corresponding percentages for 40 atm are 96.0 % : 1.1 % : 2.9 %. This suggests that pressure variation may not significantly impact relative proportions of the NOx constituents for a given $\tau_{\text{PFR-1}}$.

4. CONCLUSION

The NOx emission characteristics of an NH_3-air RQL-staged gas turbine combustor were evaluated using CRN modeling across a range of conditions representative of modern gas turbines, including variations in pressure, exit temperature, and fuel-rich stage equivalence ratio. The simulations identified the optimal stoichiometry and residence times for each stage to minimize NOx emissions while also quantifying the effects of pressure and temperature. Reaction pathway and sensitivity analyses were conducted to identify the key elementary reaction steps involved in NOx formation and reduction for the given reaction mechanism. Our results show that ammonia combustion with minimal emissions is theoretically achievable, and can enable zero-carbon power generation at low NOx emissions levels (e.g., <20 ppm) meeting site requirements with zero or minimal Selective Catalytic Reduction (SCR) cleanup.

The results of this study highlight that the residence time in PFR-1, exit temperature, rich-stage equivalence ratio, design pressure, and residence time in PFR-2 are the primary factors influencing NOx emissions at the combustor outlet. Simulations under varying exit temperature conditions indicate that selecting the residence time in PFR-2 is crucial for reducing overall NOx emissions for a given $\tau_{\text{PFR-1}}$. For a given exit temperature, NOx concentrations exhibit a slight initial decline, followed by an increase, as the residence time of PFR-2 increases. The rise in NOx concentrations with increasing PFR-2 residence time is more pronounced at higher exit temperatures. The effectiveness of high pressure in varying NOx emissions also depends on the $\tau_{\text{PFR-1}}$. For short $\tau_{\text{PFR-1}}$, the emission levels are significantly higher, and the optimal-NOx decreases with increasing design pressure. On the other hand, for long $\tau_{\text{PFR-1}}$, the emissions are substan-

tially lower, and NOx increases slightly with pressure, but the difference in optimal-NOx concentrations between the studied design pressures is minimal. For baseline conditions, NOx production/consumption are mainly controlled by HNO, NO_2, N_2O, and Zel'dovich pathways, with a notable contribution from NH_i radical reactions, particularly at higher values of ϕ_r. Sensitivity analysis highlights the importance of the kinetic rate constants of reactions involving NH_i radicals and Zel'dovich pathways under gas turbine-relevant conditions for predicting overall NOx emissions at the exit.

ACKNOWLEDGMENTS

This material is based upon work supported by the Department of Energy under Award Number DE-FE0032169.

REFERENCES

[1] Lieuwen, T. C. and Yang, V. *Gas Turbine Emissions*. Cambridge University Press, New York, NY (2013).

[2] Lefebvre, A. H. and Ballal, D. R. *Gas Turbine Combustion – Alternative Fuels and Emissions*, 3rd ed. CRC Press, Boca Raton, FL (2010).

[3] Rizk, N. K. and Mongia, H. C. "Ultra-Low NOx Rich-Lean Combustion." *Turbo Expo: Power for Land, Sea, and Air*. Paper No: 90-GT-087. 1990. American Society of Mechanical Engineers. DOI https://doi.org/10.1115/90-GT-087.

[4] Rizk, N. K. and Mongia, H. C. "NOx model for lean combustion concept." *Journal of Propulsion and Power* Vol. 11, No. 1 (1995): pp. 161–169. DOI https://doi.org/10.2514/3.23854.

[5] Nakata, T., Sato, M. O., Ninomiya, T. and Hasegawa, T. "A study on low NOx combustion in LBG-fueled 1500 °C-class gas turbine." Vol. 118 (1996): pp. 534–540. DOI https://doi.org/10.1115/1.2816680.

[6] Feitelberg, A. S. and Lacey, M. A. "The GE rich-quench-lean gas turbine combustor." Vol. 120 (1998): pp. 502–508. DOI https://doi.org/10.1115/1.2818173.

[7] Li, S., Zhang, S., Zhou, H. and Ren, Z. "Analysis of air-staged combustion of NH_3/CH_4 mixture with low NOx emission at gas turbine conditions in model combustors." *Fuel* Vol. 237 (2019): pp. 50–59. DOI https://doi.org/10.1016/j.fuel.2018.09.131.

[8] Somarathne, KD K. A., Hatakeyama, S., Hayakawa, A. and Kobayashi, H. "Numerical study of a low emission gas turbine like combustor for turbulent ammonia/air premixed swirl flames with a secondary air injection at high pressure." *International Journal of Hydrogen Energy* Vol. 42, No. 44 (2017): pp. 27388–27399. DOI https://doi.org/10.1016/j.ijhydene.2017.09.089.

[9] Kurata, O., Iki, N., Inoue, T., Matsunuma, T., Tsujimura, T., Furutani, H., Kawano, M., Arai, K., Okafor, E. C., Hayakawa, A. et al. "Development of a wide range-operable, rich-lean low-NOx combustor for NH_3 fuel gas-turbine power generation." *Proceedings of the Combustion Institute* Vol. 37, No. 4 (2019): pp. 4587–4595. DOI https://doi.org/10.1016/j.proci.2018.09.012.

[10] Okafor, E. C., Somarathne, KD K. A., Hayakawa, A., Kudo, T., Kurata, O., Iki, N. and Kobayashi, H. "Towards the development of an efficient low-NOx ammonia combustor for a micro gas turbine." *Proceedings of the Combustion Institute* Vol. 37, No. 4 (2019): pp. 4597–4606. DOI 10.1016/j.proci.2018.07.083.

[11] Stagni, A., Cavallotti, C., Arunthanayothin, S., Song, Y., Herbinet, O., Battin-Leclerc, F. and Faravelli, T. "An experimental, theoretical and kinetic-modeling study of the gas-phase oxidation of ammonia." *Reaction Chemistry & Engineering* Vol. 5, No. 4 (2020): pp. 696–711. DOI 10.1039/C9RE00429G.

[12] Kobayashi, H., Hayakawa, A., Somarathne, KD K. A. and Okafor, E. C. "Science and technology of ammonia combustion." *Proceedings of the Combustion Institute* Vol. 37, No. 1 (2019): pp. 109–133. DOI 10.1016/j.proci.2018.09.029.

[13] Rocha, R. C., Costa, M. and Bai, X.-S. "Combustion and emission characteristics of ammonia under conditions relevant to modern gas turbines." *Combustion Science and Technology* Vol. 193, No. 14 (2021): pp. 2514–2533. DOI 10.1080/00102202.2020.1748018.

[14] Gubbi, S., Cole, R., Emerson, B., Noble, D., Steele, R., Sun, W. and Lieuwen, T. "Evaluation of minimum NOx emission from ammonia combustion." *Journal of Engineering for Gas Turbines and Power* Vol. 146, No. 3 (2024): p. 031023. DOI 10.1115/1.4064219.

[15] Li, Z., Zhang, Y. and Zhang, H. "Kinetics modeling of NOx emission of oxygen-enriched and rich-lean-staged ammonia combustion under gas turbine conditions." *Fuel* Vol. 355 (2024): p. 129509. DOI 10.1016/j.fuel.2023.129509.

[16] Li, Z. and Li, S. "Kinetics modeling of NOx emissions characteristics of a NH_3/H_2 fueled gas turbine combustor." *International Journal of Hydrogen Energy* Vol. 46, No. 5 (2021): pp. 4526–4537. DOI 10.1016/j.ijhydene.2020.11.024.

[17] Goodwin, D. G., Moffat, H. K., Schoegl, I., Speth, R. L. and Weber, B. W. "Cantera: An Object-oriented Software Toolkit for Chemical Kinetics, Thermodynamics, and Transport Processes." Version 3.0.0 (2023). Accessed March 14, 2025, URL https://www.cantera.org.

[18] Glarborg, P., Miller, J. A., Ruscic, B. and Klippenstein, S. J. "Modeling nitrogen chemistry in combustion." *Progress in Energy and Combustion Science* Vol. 67 (2018): pp. 31–68. DOI 10.1016/j.pecs.2018.01.002.

[19] Powell, O. A., Papas, P. and Dreyer, C. B. "Hydrogen- and C1 – C3 Hydrocarbon-Nitrous Oxide Kinetics in Freely Propagating and Burner-Stabilized Flames, Shock Tubes, and Flow Reactors." *Combustion Science and Technology* Vol. 182, No. 3 (2010): pp. 252–283. DOI 10.1080/00102200903357724.

[20] Mei, B., Ma, S., Zhang, X. and Li, Y. "Characterizing ammonia and nitric oxide interaction with outwardly propagating spherical flame method." *Proceedings of the Combustion Institute* Vol. 38, No. 2 (2021): pp. 2477–2485. DOI 10.1016/j.proci.2020.07.133.

[21] Papas, P., Fang, R., Sung, C.-J., Smith, L. L. and Stevens, J. F. "An Assessment of Kinetic Models for Ammonia Flame Extinction." *13th U.S. National Combustion Meeting*. College Station, Texas, March 19 – 22, 2023. URL https://www.osti.gov/biblio/1957512.

[22] Fang, R., Papas, P., Sung, C.-J., Stevens, J. F. and Smith, L. L. "Effects of radiative heat loss on extinction limits of counterflow premixed ammonia-air flames." *Proceedings of the Combustion Institute* Vol. 40, No. 1-4 (2024): p. 105569. DOI 10.1016/j.proci.2024.105569.

[23] Locke, J., Kim, W., Smith, L., Snyder, T. and Dayton, J. "Operation of FT4000® Single Nozzle Combustor With High Hydrogen." *Turbo Expo: Power for Land, Sea, and Air*. Paper No: GT2024-121321. 2024. American Society of Mechanical Engineers. DOI https://doi.org/10.1115/GT2024-121321.

[24] Leonard, G. and Stegmaier, J. "Development of an Aeroderivative Gas Turbine Dry Low Emissions Combustion System." *Journal of Engineering for Gas Turbines and Power* Vol. 116, No. 3 (1994): pp. 542–546. DOI https://doi.org/10.1115/1.2906853.

[25] Glassman, I., Yetter, R. A. and Glumac, N. G. *Combustion*, 5th ed. Academic Press, Waltham, MA, USA (2015).

[26] Warnatz, J., Mass, U. and Dibble, R. W. *Combustion – Physical and Chemical Fundamentals, Modeling and Simulation, Experiments, Pollutant Formation*, 4th ed. Springer-Verlag, Berlin Heidelberg (2006).

[27] Turányi, T. and Tomlin, Alison S. *Analysis of Kinetic Reaction Mechanisms*. Springer-Verlag, Berlin Heidelberg (2014).